Biosensors and Bioelectronics 77 (2016) 116–123

Contents lists available at ScienceDirect

Biosensors and Bioelectronics

journal homepage: www.elsevier.com/locate/bios

An ultrasensitive performance enhanced novel cytochrome c biosensor for the detection of rebaudioside A

Ayyappa Bathinapatla [a], Suvardhan Kanchi [a], Parvesh Singh [b], Myalowenkosi I. Sabela [a], Krishna Bisetty [a,*]

[a] Department of Chemistry, Durban University of Technology, P.O. Box 1334, Durban 4000, South Africa
[b] School of Chemistry and Physics, University of KwaZulu Natal, Westville, Private Bag X54001, Durban 4000, South Africa

ARTICLE INFO

Article history:
Received 31 July 2015
Accepted 1 September 2015
Available online 2 September 2015

Keywords:
Rebaudioside A
Cytochrome c
Differential pulse voltammetry
Biosensor
Food samples
HOMO-LUMO calculations

ABSTRACT

In this study a novel cyctochrome c modified nanocomposite electrochemical biosensor was developed for the electrochemical determination of rebaudioside A in different food samples. The electrode surface was fabricated with graphene oxide assimilated with gold nanoparticles decorated on multiwalled carbon nanotubes/cytochrome c. The developed biosensor exhibited a 10-fold enhancement in the differential pulse voltammetry signal carried out at pH 11.0 in a 0.1 M borate buffer. Under the optimized conditions, I_p (μA) was proportional to the rebaudioside A concentration in the range of 0.001–0.05 mM (R^2=0.8308) and 0.075–1.25 mM (R^2=0.9920) with a detection limit (S/N=3) of 0.264 μM. Results of this study revealed that cyctochrome c was adsorbed tightly onto the surface of the modified electrode and showed an enzymatic catalytic activity towards the quasi-reversible reduction of rebaudioside A at −0.1 V (vs Ag/AgCl). The direct electron transfer by cytochrome c was further supported by HOMO-LUMO calculations performed at the density functional theory level. Additionally, the molecular docking simulations predicted a stronger binding affinity of rebaudioside A towards cytochrome c, thus supporting their host-guest relationship. The use of novel electrode materials in this study demonstrates the application of the electrochemical biosensor in the food industry.

1. Introduction

Rebaudioside A (Reb A) is one of the main sweetening components in steviol glycosides which are extracted from stevia rebaudiana leaves belonging to the Asteraceae family. It is also known as “Sweet-Leaf”, attracting economic and scientific interest due to the non-nutritive sweetness and the therapeutic properties of its leaf (Midmore and Rank, 2002). The acceptable daily intake (ADI) for steviol glycosides expressed by the Joint Expert Commission of Food Additions (JECFA) ranges from 2 to 4 mg kg^{-1} body weight (Geuns, 2008). Recent reports revealed that stevia leaves contain more than 35 *ent*-kaurene-type diterpene glycosides, with rebaudioside A (Reb A) and stevioside (Stv) being the most abundant (Woelwer-Rieck, 2012). The percentage (%) sweetness of the Reb A ranges from 30 to 40 which is 180–400 times sweeter than sugar. On the other hand the % sweetness of Stv ranges from 60 to 70, equivalent to 110–270 times sweeter than sugar. It is for this reason that, in addition to the pure sweetness and exceptional stability, Reb A is preferred as a sweetening component in most of the commercially available real stevia samples (Pol et al., 2007).

A literature survey of the analytical instrumentation used in the food industry revealed that high performance liquid chromatography (Woelwer-Rieck et al., 2010; Zimmermann et al., 2011; Puri et al., 2012), high performance thin layer chromatography (Jaitak et al., 2008; Londhe and Nanaware, 2013), hydrophilic interaction liquid chromatography (Well et al., 2013), liquid chromatography–mass spectrometry (Shah et al., 2012; Kakigi et al., 2013), liquid chromatography coupled to electro spray ionization mass spectrometry (Rajasekaran et al., 2008; Montoro et al., 2013) and capillary electrophoretic methods (Bathinapatla et al., 2015a) have been employed for the determination of steviol glycosides, mainly Reb A in different food samples. On the other hand electrochemical methods, in contrast have significant advantages such as faster response time, lower cost, higher sensitivity and selectivity. Lovric and co–workers reported a square wave polarographic method for the analysis of Stv in food samples (Lovric et al., 2010). Thus far there are no electrochemical or enzymatic biosensors reported for the determination of Reb A. Therefore, it is necessary to develop a biosensor with robustness, excellent catalytic activity and conductivity for the determination of Reb A.

* Corresponding author. Fax: +27 866740243.
E-mail addresses: ksuvardhan@gmail.com (S. Kanchi), bisettyk@dut.ac.za (K. Bisetty).

http://dx.doi.org/10.1016/j.bios.2015.09.004
0956-5663/

Lately, electrode modifications using nanomaterials have gained widespread interest in the selective, sensitive and reliable determination of organic compounds. In this regard, multiwalled carbon nanotubes (MWCNTs) would be useful due to their wider range of sensing applications (Ensafi and Karimi-Maleh, 2012) used for the analysis of various analytes (Eguílaz et al., 2011; Bathinapatla et al., 2015b; Xue et al., 2014; Dalkiran et al., 2014). Specifically, graphene oxide (GO), a derivative of graphene is widely used, due to the presence of a larger number of –OH, –COOH and –C–O–C– functional groups on the basal plane (Gao et al., 2013). Recently, GO was used for the fabrication of biosensors in the analysis of D– and L–tryptophan (Zor et al., 2013), dopamine and paracetamol (Cheemalapati et al., 2013), uric acid, xanthine, hypoxanthine and caffeine (Amal Raj and Abraham John, 2013), dopamine and ascorbic acid (Gao et al., 2013). Similarly, gold nanoparticles (AuNPs) have attracted much attention in the development of electrochemical biosensors. This is due to their significant properties such as high surface energy and high surface to volume ratios. AuNPs are good direct electron transfer mediators that provide enough surface area for the enzyme and protein loading capacities while retaining their bioactivity (Yang et al., 2012; Xue et al., 2014; Silva et al., 2014; Zhou et al., 2014). Cytochrome c (Cyt c), a basic redox heme-protein has been reported to play an important role in the biological respiratory chain mechanism. The direct immobilization of Cyt c onto a metal electrode surface leads to a slower electron-transfer kinetics, due to the denaturation of the proteins (Chen et al., 2009). Literature reports revealed that Cyt c can also be immobilized onto the electrode surface *via* graphene (Wu et al., 2010), AuNPs (Jensen et al., 2007), carbon nanotubes (Zhao et al., 2005) through electrostatic adsorption. This will overcome the slow electron-transfer kinetics for the determination of inorganic (Fuku et al., 2012) and organic (Xiang et al., 2013; Shervedani and Foroushani, 2014) compounds.

In this study, Cyt c immobilized on AuNPs decorated GO/MWCNTs were explored using modified platinum electrode. On comparing the pure GO and MWCNTs the combined GO/MWCNTs nanocomposite provided a higher edge density than GO and at a higher surface area than MWCNTs (Cheemalapati et al., 2013), thus enhancing the thermal stability of Cyt c activity over a wider range of pH's (Patila et al., 2013). Cyt c was adsorbed tightly on the surface of the modified electrode, showing enzyme-like activity for the reduction of Reb A. Finally, docking simulations and density functional theory (DFT) calculations were employed to get a deeper understanding of the interactions between Cyt c and Reb A at a molecular level.

2. Experiment

2.1. Chemicals and reagents

Reb A standard of 97% analytical quality were obtained from Ganzhou Julong High Tech Industrial Co., Ltd, China. The 20–30% MWCNTs basis, O.D × L 7–12 nm × 0.5–10 μm (cas no. 308068–56–6), disodium tetra borate, graphene oxide, auric chloride, ascorbic acid, sodium hydroxide, hydrochloric acid, sulfuric acid were analytical grade (Sigma Aldrich product) supplied from Capital Lab Supplies (Durban, South Africa (SA)). Horse heart cytochrome c (96%, Mw: 12,384) was obtained from Sigma and used without any further purification. Real stevia samples (containing Reb A) were purchased from a local supermarket in different forms namely; powder samples (Stevia, Dis–Chem Pty Ltd, SA), tablet samples (Green Canderel, Merisant Company 2, Czech Republic) and liquid samples (Tantalize, Delite Foods, SA). Nitrogen gas of 99.9% purity was obtained from AFROX (Durban, SA). Alumina powder ≤ 3 μm was supplied by Metrohm (Durban, SA). All solutions and samples were prepared with deionized water from an aqua MAX^{TM}–Basic 360 series water purification system supplied by TRILAB SUPPORT (Durban, SA). All standard solutions were stored at 4 °C in a refrigerator for stability.

2.2. Apparatus

Electrochemical experiments were carried out at room temperature using the previously described experimental set–up (Bathinapatla et al., 2015b). All electrochemical measurements were performed using a Metrohm model 797 VA Computrace three electrode system (Metrohm Herisau, Switzerland) consisting of the platinum electrode as the working electrode, the reference electrode was Ag/AgCl and the platinum wire was used as the counter electrode. All the solutions examined were initially purged with purified nitrogen gas for 10 min. The pH measurements were carried out on a CRISON micro pH 2000 digital pH meter using a combined electrode (glass electrode-reference electrode) with an accuracy of ± 0.1 pH units. Morphology studies were carried out using the transmission electron microscope (TEM) model JEM 2100 equipped with a LaB_6 emitter (MAX OXFORD instruments). UV–vis absorption spectra for GO and AuNPs decorated MWCNTs/GO studies were performed using a UV2450 spectrophotometer (Shimadzu). The STAR^e system of TGA/DCS 1 SF/1346 model supplied with a STAR^e software version 9.20 by METTLER TOLODO (Johannesburg, SA) was used for the thermogravimetric analysis. Compositional and phase identification was performed on an X-ray diffractometer D8 Advance equipped with a Co-Kα radiation, operated at 35 mV and 30 mA. The measurements were taken with 2 Theta (2θ) angle ranging from 5 to 90°, with a scanning rate of 0.02 S^{-1}. The recorded X-ray diffractograms were processed using Eva/Origin software. All solutions were sonicated using an ultrasonicator (Labcon 5019 U model).

2.3. Preparation of standard, supporting electrolyte and samples

Reb A standard solution (0.1 mM) was prepared quantitatively by weighing an equivalent amount in a 5.0 mL volumetric flask and diluted with deionized water up to the calibration mark. Likewise, 0.1 M borate buffer was prepared from disodium tetra borate in 100 mL of distilled water. The optimum pH 11.0 was achieved by quantitatively adding NaOH/HCl and thereafter solutions were stored at 4 °C. The cleaning of all the samples prior to voltammetric measurements were done with a disposable syringe fitted with a 0.45 μm pore size and 25 mm diameter cellulose filter (Anatech Instruments (Pty) Ltd.). For sample analysis, 0.140 g (Stevia) powdered and 0.165 g Green Canderel (tablet) samples were directly dissolved in 10 mL deionized distilled water respectively. The (Tantalize) liquid sample was diluted with 1:10 (v/v) ratio prior to electrochemical measurements.

2.4. Preparation and fabrication of Cyt c/AuNPs-GO/MWCNTs nanocomposite

The AuNPs dispersed in water were prepared in a 100 mL flat bottom flask as follows. Approximately 50 mL of 0.01% $HAuCl_4$ solution was boiled with vigorous stirring and 50 mM ascorbic acid was added drop wise until a color changed from pale yellow to blue. The color change persisted until a red–violet appeared within 60 s and solution allowed to boil while stirring for another 10 min. AuNPs decorated with GO were prepared by dissolving 1 mL of GO in 10 mL of deionized water. To this solution 5 mL of the previously prepared AuNPs solution was added and then ultrasonicated for 1 h to obtain AuNPs-GO material. For the preparation of AuNPs-GO/MWCNTs nanocomposite, MWCNTs were added to the 5 mL of AuNPs-GO solution and then sonicated for

45 min to produce a homogenous dispersion of AuNPs-GO/MWCNTs (Cheemalapati et al., 2013). Finally, the resulting AuNPs-GO/MWCNTs dispersion was centrifuged at 3000 rpm to separate the loosely bound MWCNTs and washed several times with deionized water. The resultant black residue was used to fabricate the Pt electrode. This was achieved by manually polishing the bare Pt electrode to a mirror like surface with an alumina slurry (≤ 3 μm) and then rinsed with distilled water. Thereafter, it was electrochemically cleaned at a potential ranging from −0.4 to 1.0 V for 30 cycles in acidified distilled water. This process enabled the removal of any physi-sorbed or chemi-sorbed materials from the electrode surface. Thereafter, the Pt electrode was coated by careful immobilization of different nanocomposites (in three stages) to evaluate the electron transfer kinetics. In the first stage, 6.0 μL of AuNPs-GO material was coated on the Pt electrode and dried at 50 °C for 10 min to prepare AuNPs-GO/Pt. For the second stage, 6.0 μL of AuNPs-GO/MWCNTs material was coated and dried for 10 min at 50 °C. Finally, AuNPs-GO/MWCNTs modified Pt electrode was dipped in 1.0 mg mL^{-1} of Cyt c solution for 12 h at 4 °C and then dried at room temperature for another 15 min. As a result Cyt c was adsorbed onto the nanocomposite and the fully fabricated (Cyt c/AuNPs-GO/MWCNTs/Pt) electrode was ready for use.

2.5. Electrochemical measurements with Cyt c/AuNPs-GO/MWCNTs/Pt electrode

Approximately 10 mL of the borate buffer (pH 11.0) was introduced into the electrochemical cell in which either bare Pt or fabricated Pt electrode was immersed. Several cyclic sweeps were applied until a low background current was achieved. An aliquot of the analyte solution was then introduced into the electrochemical cell, and a pre-concentration potential was applied to the working electrode while the solution was stirred at 400 rpm. At the end of the pre-concentration step, stirring was stopped and a 5 s equilibration period was allowed for the solution to become quiescent. The voltammograms were then recorded using the bare Pt or the modified Pt electrode by scanning the potential towards the positive direction using differential pulse or linear sweep potential at a scan rate of 0.1 V/s.

3. Results and discussion

3.1. Characterization of Cyt c/AuNPs-GO/MWCNTs/Pt electrode

Microscopic images in Fig 1 revealed potential modifications on the surface of the AuNPs-GO/MWCNTs nanocomposite. Fig. 1A shows the characteristic morphology of pure MWCNTs with a clear hollow cylindrically shaped shells, while in Fig. 1B ultra-thin sheets of pure GO with a diameter of nano to sub-micro meter are observed. The TEM image of GO/MWCNTs nanocomposite in Fig. 1C illustrates that the MWCNTs are well incorporated with ultra-thin sheets of GO due to π–π interactions between the side walls of MWCNTs and the hydrophilic functionalities of GO. In Fig. 1D–E the AuNPs are well distributed in a uniform size on the GO thin sheet and the outer surface of the MWCNTs. The EDS results showed that the coated AuNPs have an even distribution on the surfaces and tendency of aggregation reduced due to the hydrophilic functionalities of GO.

The crystalline characterization of the AuNPs-GO/MWCNTs nanocomposite performed by XRD are shown in Fig. 1F. The

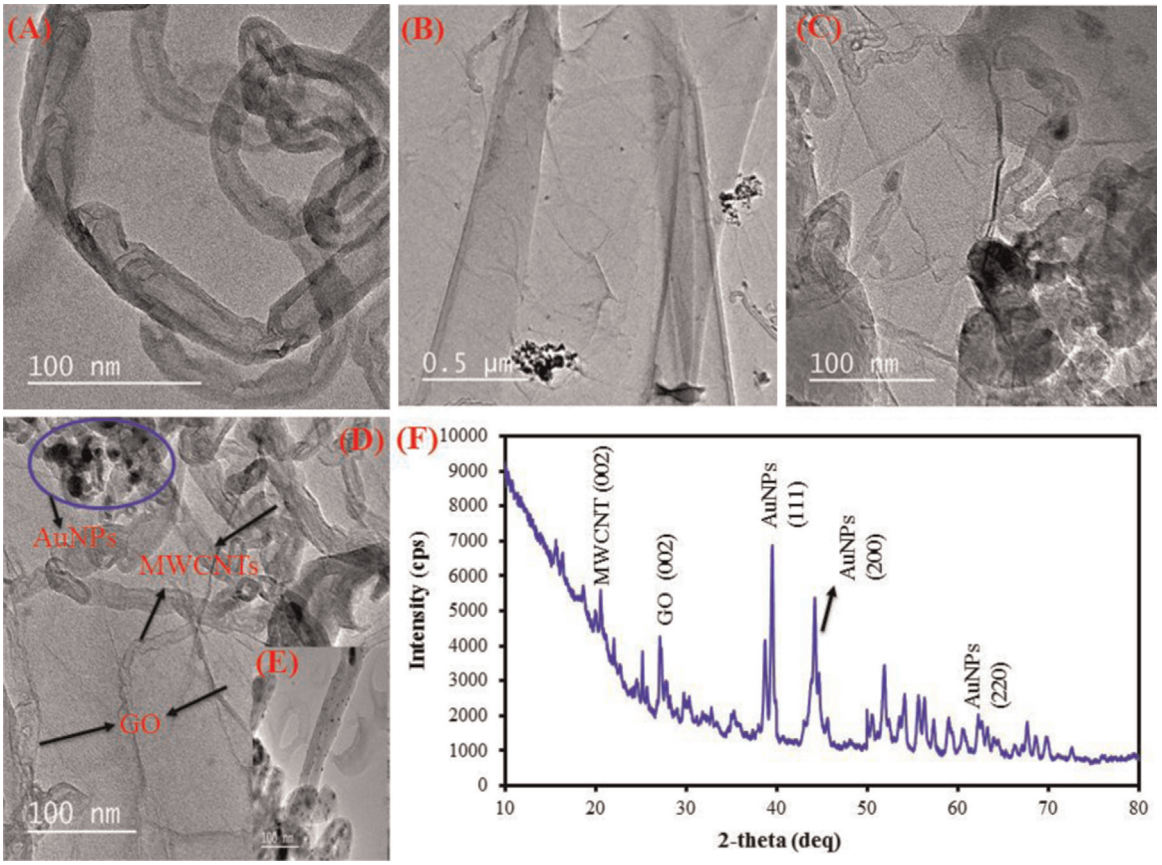

Fig. 1. TEM images for (A) pure MWCNTs (B) pure GO (C) MWCNTs on the surface of GO (D and E) AuNPs decorated on MWCNTs and GO surface (F) XRD patterns of AuNPs fabricated GO/MWCNTs nanocomposite.

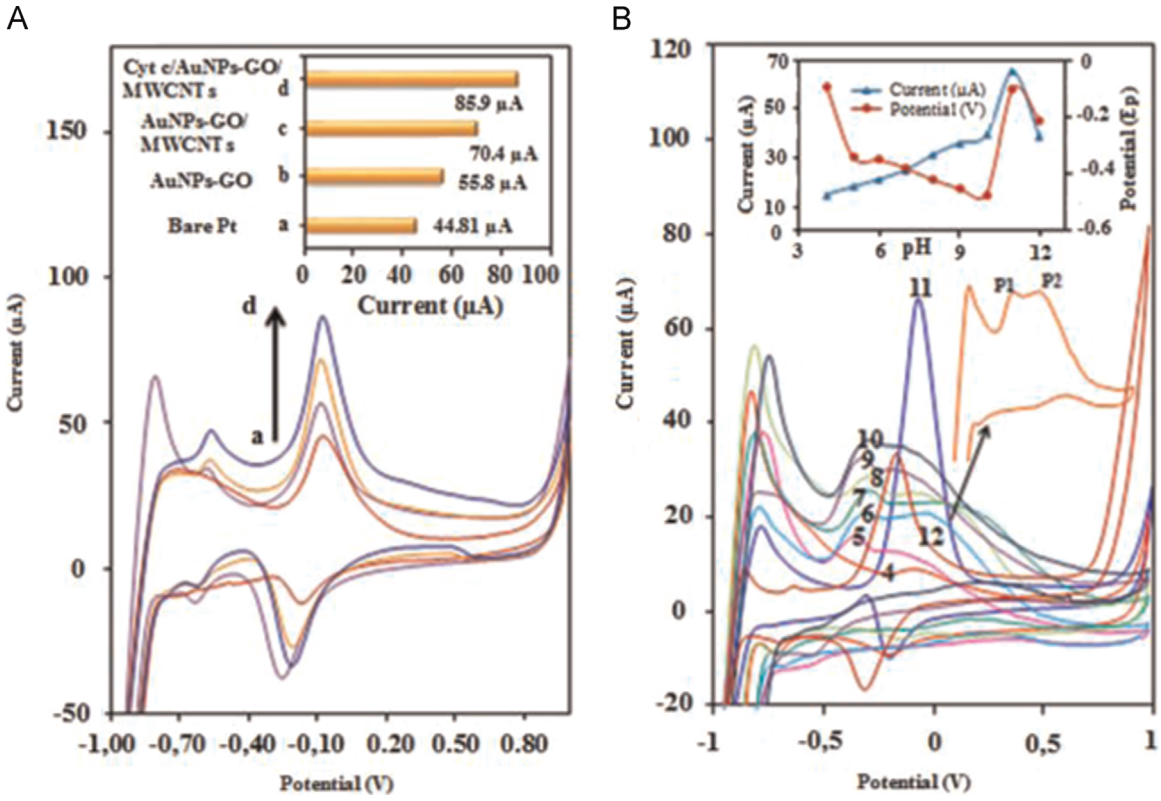

Fig. 2. (A) Cyclic voltammograms recorded at (a) bare Pt (b) AuNPs-GO modified Pt (c) AuNPs-GO/MWCNTs modified Pt (d) Cyt c/AuNPs-GO/MWCNTs modified Pt (B) Cyclic voltammograms recorded at different pHs (4.0 to 12.0) with 0.3 mM Reb A, scan rate 70 mV s^{-1} and in inset shows the effect of pH on peak current and potentials.

diffraction peaks observed around $2\theta = 23°$ and 27° were assigned to the (002) plane of carbon materials such as MWCNTs and GO respectively (Prabakaran and Pandian, 2015). All the other peaks, $2\theta = 39°$, 44.6° and 64.7° were assigned to the Au planes of (111), (200) and (220) respectively (Li et al., 2015). According to the Scherrer and Williamson–Hall formula, the calculated average particle size of the AuNPs in the nanocomposite ranging from 10–33 nm for different peaks and the average crystalline size was found to be 23.7 nm with a face-centered-cubic (FCC) crystal structure.

Furthermore, the nanocomposites were characterized by UV–vis spectroscopy and the results showed that GO exhibited two characteristic peaks at 230 mm and a broader peak at 311 nm associated with π–π* and n–π* transitions respectively. While, AuNPs-GO/MWCNTs composite also exhibited two similar peaks, but the positions of π–π* peaks bathochromically shifted to 262 nm respectively. This confirmed the formation of the π–π interactions between the side walls of MWCNTs and the AuNPs of GO as shown in Fig. S1A.

The thermal behavior and stability of the prepared nanocomposites were investigated by thermogravimetric analysis (TGA). Fig. S1B showed the TGA curves for MWCNTs (curve i), GO (curve ii), GO/MWCNTs composite (curve iii) and AuNPs-GO/MWCNTs composite (curve iv). MWCNTs showed two significant decrements in the mass around 322 and 650 °C. In the first peak, a 6% weight loss was observed due to the evaporation of the total moisture content and the second decrease was due to the oxidation of carbon into gaseous carbon dioxide in the temperature range of 450–680 °C and the calculated weight loss was 11%. GO started to lose weight from 60 °C and the main weight loss took place around 90 °C with a total weight loss of 98%. These weight loses were due to the pyrolysis of the labile oxygen atoms containing functional groups such as -OH, -COOH to CO, CO_2 and steam (Pham et al., 2011). The TGA curve for GO-MWCNTs composite showed two significant drops around 100-258 °C and 420-560 °C. In the first zone, there is 8.86% weight loss that which can be attributed to the oxidation of the GO functionalities. The second weight loss of 5.2% corresponds to the MWCNTs, indicating the thermal stability of GO increased in the presence of MWCNTs, due to the incorporation of MWCNTs with GO. The AuNPs-GO/MWCNTs composite thermogram shows two significant mass drops at 319 °C and 510 °C with a weight loss of 19%. The percentage of AuNPs loaded onto the surface of GO/MWCNTs was found to be 27%. Consequently, the presence of AuNPs increased the thermal stability of the nanocomposites (Jia et al., 2013).

3.2. Electrochemical characterization of the developed sensor and Reb A behavior towards Cyt c/AuNPs-GO/MWCNTs/Pt

The microscopic areas of the developed biosensor was characterized using cyclic voltammetry (CV) with 1.0 M $K_3Fe(CN)_6$ as a probe solution. The $[Fe(CN)_6]^{3-}$ showed heterogeneous one-electron transfer ($n=1$) reaction, one of the most broadly studied redox couples in electrochemistry. The anodic and cathodic peak currents of $[Fe(CN)_6]^{3-}$ reaction linearly increased, while the peak potentials of the anodic and cathodic peaks shifted to positive and negative sides with an increase in scan rates from 10 to 210 mV/s. The microscopic areas for the bare and modified Pt electrodes were studied using Randles–Sevcik equation (Bathinapatla et al., 2015b).

$$I_{pa} = 2.69 \times 10^5 A C_o n^{3/2} D_R^{1/2} v^{1/2} \quad (1)$$

Where I_P refers to the peak current, A is the surface area of the electrode, C_o is concentration of the $K_3Fe(CN)_6$, n is the number of electrons transferred, D_R is the diffusion coefficient and v is the scan rate. The diffusion coefficient (D_R) of 6.7×10^{-6} cm^2 s^{-1} was calculated from the slope of the $I_{pc} - v^{1/2}$ graph. In the case of Cyt

c/AuNPs-GO/MWCNTs/Pt, the electrode surface area was calculated as 0.842 cm^2, while the bare Pt electrode were nearly six times smaller than the modified electrode.

The electrochemical performance of Cyt c/AuNPs-GO/MWCNTs/Pt for the detection of Reb A in food samples were studied by measuring the current-potential responses. The calculated microscopic areas of the electrodes were mainly effected by the peak responses of Reb A. Therefore, a comparative study among various modified electrodes were studied on peak currents (i_{pa}) using CV in a 10 mL borate buffer (pH 11.0) at a scan rate of 70 mV s^{-1}. The peak currents were directly proportional to the coating of the electrode material, due to an increase in electro active surface area. Fig. 2A shows the electrochemical responses of Reb A at −0.1 V (vs Ag/AgCl) with the bare Pt (curve a), AuNPs-GO/Pt (curve b) AuNPs-GO/MWCNTs/Pt (curve c) and Cyt c/AuNPs-GO/MWCNTs/Pt (curve d).

The bare Pt electrode (curve a) showed a broad and weak intensity peak due to the slower electron transfer kinetics of the reduction process. In contrast, well-defined sharp peaks were observed with fair responses for the different modified electrodes. The bar graphs (inset Fig. 2A) showed comparative current responses of the four electrodes studied, clearly indicating that the peak currents by Cyt c/AuNPs-GO/MWCNTs/Pt (85.9 μA) were significantly higher than that of the bare Pt (44.81 μA) electrode, AuNPs-GO/Pt (55.8 μA) and AuNPs-GO/MWCNTs/Pt (70.4 μA). The peak currents obtained with GO and MWCNTs alone on the Pt electrode were in the range of bare Pt electrode, hence AuNPs-GO/Pt and AuNPs-GO/MWCNTs/Pt systems were tested for further evaluation. AuNPs alone are difficult to coat on the bare Pt electrode for the electron transfer testing, hence GO and MWCNTs were coated as a platform to load AuNPs. The addition of Cyt c on AuNPs-GO/MWCNTs/Pt showed excellent catalytic activity towards reduction of Reb A, by improving the peak currents. Considering the structure of Reb A, the electrode reaction attributed to the reduction of the carboxyl groups with a one electron transfer (Scheme 1), resulting in the appearance of a quasi-reversible reduction peak at −0.1 V (versus Ag/AgCl) (Lovric et al., 2010). Similar types of reactions were also observed in the case of cocaine (Pavlova et al., 2004), nalidixic acid (Ibrahim et al., 2002).

3.3. Effect of pH and scan rate on the peak currents and peak potentials

A 0.3 mM Reb A solution was used to find the optimum pH of the supporting electrolyte by Cyt c/AuNPs-GO/MWCNTs/Pt. The effect of pH ranging from 4.0 to 12.0 on the reduction peak currents of Reb A were studied in a 0.1 M borate buffer using CV. According to Fig. 2B, the pH of the electrolyte increases with an increasing peak current until a maximum of 85.9 μA at pH 11.0, due to the higher electron transfer between the modified electrode and Reb A.

The effect of pH on the peak potentials were also investigated and depicted in Fig. 2B. The peak potentials were mainly pH dependent, due to the reduction capacity of the carboxylic group. It was also observed that the peak potentials shifted towards a more negative value with an increase in pH. Interestingly from pH 4.0 to 9.0, two peaks were observed in the voltammogram (indicated as P1 and P2). The first peak related to the reduction of the carboxyl group and the second peak corresponds to hydrogen evolution which interfered with the negatively charged oxygen in the acidic medium. However, in a more basic medium 10.0 to 12.0, the appearance of second peak decreased and merged as a single broad peak, due to a decrease in the effect of the hydrogen evolution. Thus, based on the peak currents and the less negative potentials, the 0.1 M borate buffer at pH 11.0 was considered as the optimum for determination of Reb A. The rest of the data on the two independent parameters, scan rate and accumulation time are discussed in supplementary data for the effect on peak current and peak potentials.

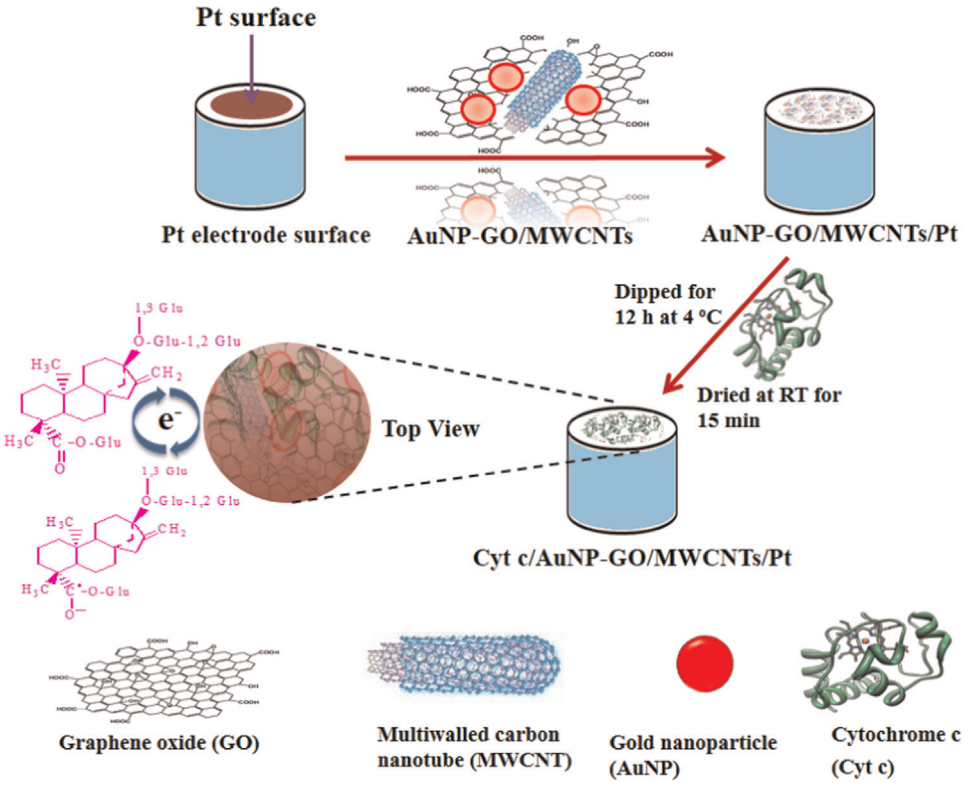

Scheme 1. Fabrication of Pt electrode with nanocomposite and electrochemical mechanism for Reb A.

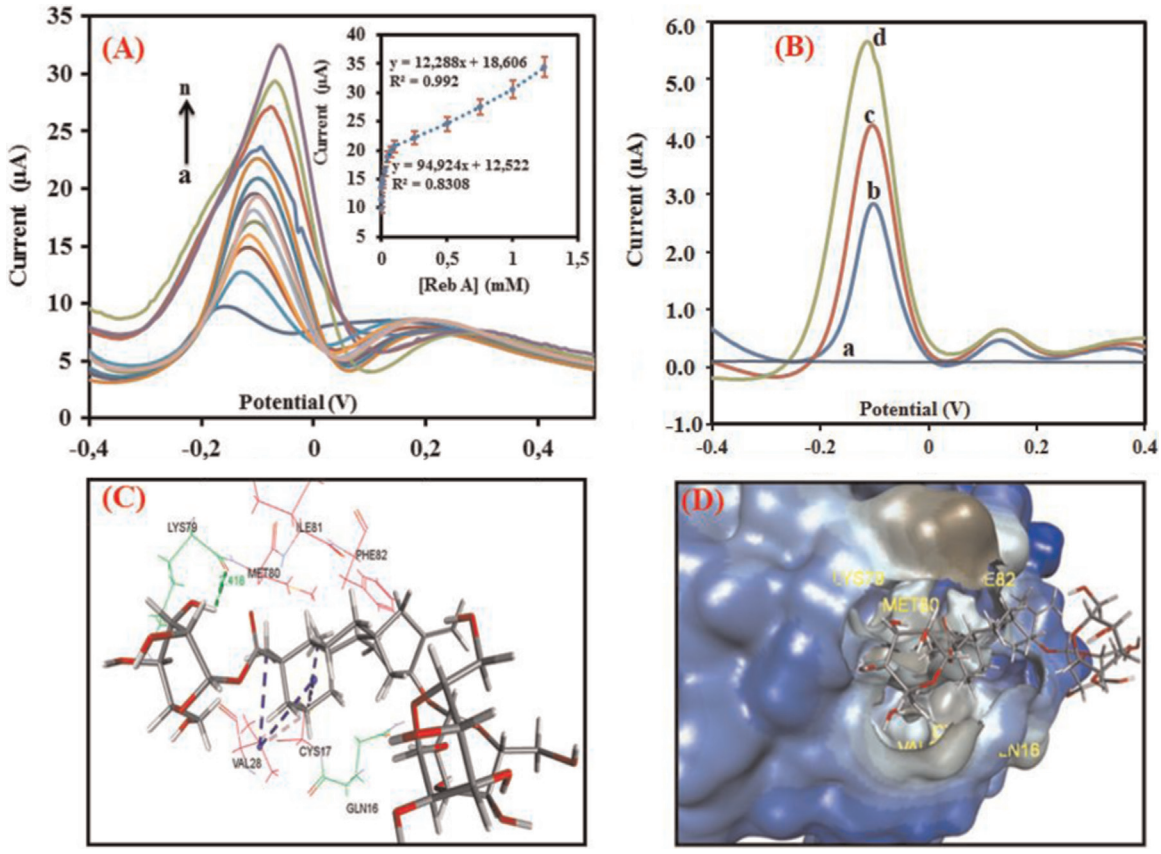

Fig. 3. (A) Typical DPVs of (a) 0.001(b) 0.0025 (c) 0.005 (d) 0.0075 (e) 0.01 (f) 0.025 (g) 0.05 (h) 0.075 (i) 0.1 (j) 0.25 (k) 0.5 (l) 0.75 (m) 1 (n) 1.25 mM for Reb A in 0.1 M borate buffer (pH 11.0) and in inset calibration plot of *Ip* vs [Reb A] at low (0.001 to 0.05) and high (0.075 to 1.25) concentrations (B) Overlay of DPVs for 200 μL of (a) blank (b) powder (c) tablet and (d) liquid samples (C) Conformation of Reb A (in sticks format) docked into the active site of Cyt c. Only interacting amino acid (AA) residues (in lines format) were shown. Hydrophobic and hydrophilic AA were shown in magenta and green color lines. Hydrogen bonding is shown as green dotted line, whereas hydrophobic interactions are depicted in blue dotted lines (D) Surface representation of Cyt c (a side view) showing the presence of a groove responsible for the penetration of Reb A (shown in sticks format) into its active site.

3.4. DPV method for quantitative determination of Reb A

The DPV response for various concentrations of Reb A at the modified electrode in a 0.1 M borate buffer were measured under the optimum experimental conditions (pH 11.0, accumulation time: 30 s, accumulation potential: −30 mV, pulse amplitude: 50 mV, voltage step: 2 mV and voltage step time: 0.4 s). The results showed a linear relationship between the concentration ranging from 0.001 to 1.25 mM of Reb A and the peak currents, as depicted in Fig. 3A. Under the optimized conditions, I_{pa} (μA) was proportional to the Reb A concentration in two concentration ranges (Fig. 3A), shown in Eqs. (2 and 3) below:

(1) First linear dynamic range (LDR): 0.001–0.05 mM

$$I_{pa}(\mu A) = 94.924\ C + 12.52 (R^2 = 0.8308) \quad (2)$$

(2) Second linear dynamic range (LDR): 0.075–1.25 mM

$$I_{pa}(\mu A) = 12.28\ C + 18.60 (R^2 = 0.9920) \quad (3)$$

with 0.264 μM of LOD and 0.752 μM of LOQ at a signal to noise ratio of 3. A break in the calibration curve of Reb A probably reflects the formation of a sub-monolayer in the first range and the formation of a monolayer in the second range of the calibration plot (Kachoosangi et al., 2008; Sanghavi et al., 2014). The obtained detection limits were compared with the reported methods as shown in Table S1 and the results suggests that the developed sensor is ultrasensitive for the determination of Reb A in food samples.

3.5. Stability, recovery, accuracy and precision studies

The stability and repeatability of the developed biosensor were tested using CV which resulted in a decrease of 3.6% of the current response after 50 cycles. The long term stability of the developed sensor was observed by measuring the response in 0.3 mM Reb A for ten replicate measurements ($n=10$) over three consecutive days using the same coating. The sensor maintained 89% of its original response by the third day, hence its activity was retained to a large extent. The analytical parameters in terms of accuracy, precision and recovery were estimated by analysing standard solutions of Reb A with three different concentrations ranging from 0.1 to 0.7 mM in a day ($n=3$). The relative error (bias) was observed from −0.1300 to −0.0214 with a % RSD of 0.93 to 1.26, indicating a higher accuracy and precision of the proposed method

Table 1
Analytical parameters (stability, accuracy, precision and recovery ($n=3$)) obtained for Reb A at Cyt c/AuNPs-GO/MWCNTs/Pt.

Stability		Analytical parameters				
Day	Peak responce[a] (I_p)	Added (mM)	Found (mM)	Bias[a]	Recovery (%)	RSD[c] (%)
1	81	0.10	0.087	−0.1300	87.0	1.32
2	76	0.40	0.391	−0.0225	97.0	0.93
3	72	0.70	0.685	−0.0214	98.0	1.26

Bias=(found-added/added).

[a] Average of three individual determinations.

[c] Relative standard deviation for three individual determinations.

Table 2
Detection of the Reb A in different food samples.

Sample (Type)	Sample in 10 mL water	Reb A (mg mL^{-1}), (m/m%)	RSD[d]
Stevia[a] (Powder)	0.140 g	9.58 (68%)	1.57
Green Canderel[b] (Tablet)	0.165 g	13.28 (81%)	1.59
Tantalize[c] (Liquid)	1.0 mL	15.80 (87%)	1.83

[a] Dis-Chem Pty Ltd, South Africa.
[b] Merisant Company 2, Sarl, Czech Republic.
[c] Delite Foods, South Africa.
[d] Relative standard deviation for three individual determinations.

(Table 1). On the other hand percentage recoveries of the proposed sensor ranged from 87.0 to 98.0% at same concentrations. The reproducibility of the biosensor was confirmed by further assaying of the CV peak currents using 0.3 mM Reb A at the three prepared electrodes, resulting in the % RSD of 1.57 obtained for the three replicate measurements.

3.6. Real sample analysis and interference study

Finally, the performance of the developed biosensor was tested for the analysis of Reb A in three commercially available food samples as illustrated in Fig. 3B. The quantitative results in Table 2 corresponds to the mean voltammogram for the triplicate analysis of Reb A in a tablet, powder and liquid samples. The percentage recoveries were calculated for the mass of Reb A per mass of the tablet (81%), for the powder sample (68%) and 87% for the liquid samples. Understandably, the difference in the quantity may arise from the fact that these samples are not exactly the same or pure as they are from various origins.

Furthermore, the selectivity of the biosensor was studied by detecting 0.3 mM Reb A solution in the presence of several possible co-existing interferences such as aspartame, acesulfame K, nitrate, cocaine, nalidixic acid, fenofibrate and benzoylecgonine. Using the current ratio method, the degree of substance interfered with Reb A was evaluated. The current ratio of 0.3 mM Reb A in the presence of 1.0 mM of different interfering substances (I_{R+S}) were calculated and compared with the peak current of 0.3 mM Reb A alone (I_R). The current ratios (I_{R+S}/I_R) were 0.98, 1.01, 0.97, 0.89, 0.95, 0.93, 0.89 and 0.92 obtained for each of above mentioned co-existing interferences respectively. Since there were no significant changes in the current ratio, our results confirm that the developed biosensor exhibited an excellent selectivity towards the Reb A.

3.7. Docking analysis and HOMO-LUMO calculations

Docking simulations between Cyt c and Reb A were performed using the CDocker module (Wu et al., 2003) embedded in Discovery Studio. The computed scoring function (CDocker interaction energy: −25.7) indicated that the Reb A fits tightly in the active site of the Cyt c. The computed binding energy $[E_{complex}-(Energy_{ligand}+Energy_{protein})]$ around −106.7 kcal mol^{-1} further corroborated the strong binding affinity of Reb A to Cyt c. The docked complex of Cyt c and Reb A were subsequently visualized to get a deeper understanding of their host-guest relationships and is pictorially shown in Figs. 3C–D (for details see Supplementary data). Both hydrogen bonding and hydrophobic forces were found to responsible for stabilization of their complex. Additionally, HOMO-LUMO calculations were also used to identify the exact positions of the oxidation or reduction reactions in a molecule with the help of electron density maps (see Supplementary data).

4. Conclusions

In the present work, a novel Cyt c modified nanocomposite electrochemical biosensor was developed for the determination of Reb A in different food samples. The developed biosensor was characterized by UV–vis, EDS, TEM and TGA techniques. Additionally, the electrochemical behavior of the biosensor was evaluated using CV and DPV. Our results indicated that the Cyt c/AuNPs-GO/MWCNTs/Pt exhibited efficient electrocatalytic reduction for Reb A with a relative ultra-sensitivity and stability. Under the optimized conditions, the first LDR was from 0.001–0.05 mM while second ranged from 0.075–1.25 mM, with a detection limit of 0.264 μM for the Reb A. The applicability of the biosensor was tested with real food samples, and the good performance of the Cyt c/AuNPs-GO/MWCNTs/Pt provided a promising alternative in routine sensing applications of Reb A in the food industry. Docking simulations further revealed that Reb A has a stronger tendency to bind with Cyt c *via* hydrogen bonding and hydrophobic interactions. HOMO-LUMO calculations were helpful for the prediction of the most appropriate functional groups or atoms undergoing oxidation or reduction reactions. The developed Reb A electrochemical biosensor is a first of its kind and along with its superior qualities like sensitivity, selectivity and reproducibility, needless to say that it has the potential to pave the way at an industrial level with its promising applicability.

Acknowledgments

The research has been carried out with financial support from the Durban University of Technology and National Research Foundation of South Africa. The authors would like to express their acknowledgment to the Centre for High Performance Computing, an initiative supported by the Department of Science and Technology of South Africa.

Appendix A. Supplementary material

Supplementary data associated with this article can be found in the online version at http://dx.doi.org/10.1016/j.bios.2015.09.004.

References

Amal Raj, M., Abraham John, S., 2013. Anal. Chim. Acta 771, 14–20.
Bathinapatla, A., Kanchi, S., Singh, P., Sabela, M.I., Dovey, M., Bisetty, K., 2015a. J. Iran. Chem. Soc. 12, 127–136.
Bathinapatla, A., Kanchi, S., Singh, P., Sabela, M.I., Bisetty, K., 2015b. Biosens. Bioelectron. 67, 200–207.
Cheemalapati, S., Palanisamy, S., Mani, V., Chen., S.M., 2013. Talanta 117, 297–304.
Chen, X., Long, H.Y., Wu, W.L., Yang, Z.S., 2009. Thin Solid Films 517, 2787–2791.
Dalkiran, B., Kacar, C., Erden, P.E., Kilic, E., 2014. Sensor Actuator B 200, 83–91.
Eguílaz, M., Villalonga, R., Agüí, L., Sedeño, P.Y., Pingarrón, J.M., 2011. J. Electroanal. Chem. 661, 171–178.
Ensafi, A.A., Karimi-Maleh, H., 2012. Drug Test. Anal. 4, 970–977.
Fuku, X., Iftikar, F., Hess, E., Iwuoha, E., Baker, P., 2012. Anal. Chim. Acta 730, 49–59.
Gao, F., Cai, X., Wang, X., Gao, C., Liu, S., Gao, F., Wang, Q., 2013. Sensor Actuator B 186, 380–387.
Geuns, J.M.C., 2008. Proceedings of the 2nd Stevia Symposium. Leuven, 59–78.
Ibrahim, M.S., Shehatta, I.S., Sultan, M.R., 2002. Talanta 56, 471–479.
Jensen, P.S., Chi, Q., Grumsen, F.B., Abad, J.M., Horsewell, A., Schiffrin, D.J., Ulstrup, J., 2007. J. Phys. Chem. C 111, 6124–6132.
Jaitak, V., Gupta, A.P., Kaul, V.K., Ahuja., P.S., 2008. J. Pharm. Biomed. Anal 47, 790–794.
Jia, Y., Yu, K., Qian, K., 2013. Nanoscale Res. Lett. 8 (243), 1–6.
Kachoosangi, R.T., Wildgoose, G.G., Compton, R.G., 2008. Anal. Chim. Acta 618, 54–60.
Kakigi, Y., Suzuki, T., Icho, T., Uyama, A., Mochizuki, N., 2013. Food Addit. Contam. A 30, 2043–2049.
Li, X., Wang, X., Li, L., Duan, H., Luo, C., 2015. Talanta 131, 354–360.
Londhe, S.V., Nanaware, S.M., 2013. J. AOAC Int. 96, 24–26.

Lovric, S.K., Novak, I., Novak, B., 2010. Electroanalysis 22, 2211–2215.
Midmore, D.J., Rank, A.H., 2002. Publication No. W02/022 RIRDC Project No.UCQ-16A.
Montoro, P., Molfetta, I., Maldini, M., Ceccarini, L., Piacente, S., Pizza, C., Macchia, M., 2013. Food Chem. 141, 745–753.
Patila, M., Pavlidis, I.V., Diamanti, E.K., Katapodis, P., Gournis, D., Stamatis, H., 2013. Process Biochem. 48, 1010–1017.
Pavlova, V., Mirceski, V., Lovric, Š.K., Jovanovic, S.P., Mitrevski., B., 2004. Anal. Chim. Acta 512, 49–56.
Pham, T.A., Choi, B.C., Lim, K.T., Jeong, Y.T., 2011. Appl. Surf. Sci. 257, 3350–3357.
Prabakaran, E., Pandian, K., 2015. Food Chem. 166, 198–205.
Pol, J., Vostra, E.V., Karasek, P., Roth, M., Benesova, K., Kotlarikova, P., Caslavsky, J., 2007. Anal. Bioanal. Chem. 388, 1847–1857.
Puri, M., Sharma, D., Barrow, C.J., Tiwary, A.K., 2012. Food Chem. 132, 1113–1120.
Rajasekaran, T., Ramakrishna, A., Sankar, K.U., Giridhar, P., Ravishankar, G.A., 2008. Food Biotechnol. 22, 179–188.
Sanghavi, B.J., Kalambate, P.K., Karna, S.P., Srivastava, A.K., 2014. Talanta 120, 1–9.
Shah, R., Jager, L.S.D., Begley, T.H., 2012. Food Addit. Contam. A 29, 1861–1871.
Shervedani, R.K., Foroushani, M.S., 2014. Bioelectrochem 98, 53–63.
Silva, P.S., Gasparini, B.C., Magosso, H.A., Spinelli., A., 2014. J. Hazard. Mater. 273, 70–77.
Well, C., Frank, O., Hofmann, T., 2013. J. Agric. Food Chem. 61, 11312–11320.
Woelwer-Rieck, U., 2012. J. Agric. Food Chem. 60, 886–895.
Woelwer-Rieck, U., Lankes, C., Wawrzun, A., Wust, M., 2010. Eur. Food Res. Tech. 231, 581–588.
Wu, J.F., Xu, M.Q., Zhao, G.C., 2010. Electrochem. Commun. 12, 175–177.
Wu, G., Robertson, D.H., Brooks III, C.L., Veith, M., 2003. J. Comp. Chem. 24, 1549–1562.
Xiang, C., Zou, Y., Qiu, S., Sun, L., Xu, F., Zhou, H., 2013. Talanta 110, 96–100.
Xue, C., Wang, X., Zhu, W., Han, Q., Zhu, C., Hong, J., Zhou, X., Jiang, H., 2014. Sensor Actuator B 196, 57–63.
Yang, L., Liu, S., Zhang, Q., Li, F., 2012. Talanta 89, 136–141.
Zhao, G.C., Yin, Z.Z., Zhang, L., Wei, X.W., 2005. Electrochem. Commun. 7, 256–260.
Zhou, Y., Dong, H., Liua, L., Li, M., Xiao, K., Xu, M., 2014. Sensor Actuator B 196, 106–111.
Zimmermann, B.F., Woelwer-Rieck, U., Papagiannopoulos, M., 2011. Food Anal. Method 5, 266–271.
Zor, E., Patir, I.H., Bingol, H., Ersoz, M., 2013. Biosens. Bioelectron. 42, 321–325.